

RESEARCH ARTICLE | SEPTEMBER 15 2022

A frequency comb stabilized Ti:Sa laser as a self-reference for ion-trap experiments with a $^{40}\text{Ca}^+$ ion

F. Domínguez; J. Bañuelos; J. Berrocal; ... et. al



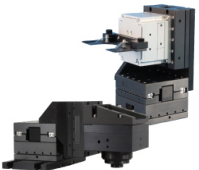
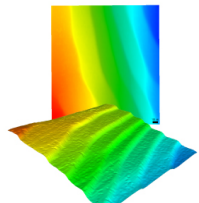
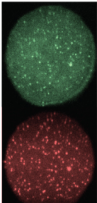


Rev Sci Instrum 93, 093304 (2022)

<https://doi.org/10.1063/5.0094452>



CrossMark

 <p>MCL MAD CITY LABS INC. www.madcitylabs.com</p>	<p>Nanopositioning Systems</p> 	<p>Modular Motion Control</p> 	<p>AFM and NSOM Instruments</p> 	<p>Single Molecule Microscopes</p> 
---	--	--	---	--

A frequency comb stabilized Ti:Sa laser as a self-reference for ion-trap experiments with a $^{40}\text{Ca}^+$ ion

Cite as: Rev. Sci. Instrum. 93, 093304 (2022); doi: 10.1063/5.0094452

Submitted: 3 April 2022 • Accepted: 15 August 2022 •

Published Online: 15 September 2022







View Online



Export Citation



CrossMark

F. Domínguez,¹  J. Bañuelos,^{1,a)} J. Berrocal,¹  J. J. del Pozo,¹  M. Hernández,^{1,b)}  A. Carrasco-Sanz,² J. Cerrillo,³  P. Escobedo-Araque,^{4,c)}  and D. Rodríguez^{1,5,d)} 

AFFILIATIONS

¹Departamento de Física Atómica, Molecular y Nuclear, Universidad de Granada, 18071 Granada, Spain

²Departamento de Óptica, Universidad de Granada, 18071 Granada, Spain

³Área de Física Aplicada, Universidad Politécnica de Cartagena, 30202 Cartagena, Spain

⁴Bendable Electronics and Sensing Technologies (BEST) Group, University of Glasgow, G12 8QQ Glasgow, United Kingdom

⁵Centro de Investigación en Tecnologías de la Información y las Comunicaciones, Universidad de Granada, 18071 Granada, Spain

^{a)}Present address: ALBA Synchrotron Light Source, 08290 Cerdanyola del Vallès, Barcelona, Spain.

^{b)}Present address: ICFO - Institut de Ciències Fotoniques, The Barcelona Institute of Science and Technology, Castelldefels, Barcelona 08860, Spain.

^{c)}Present address: ECsens, CITIC-UGR, Departamento de Electrónica y Tecnología de Computadores, Universidad de Granada, 18071 Granada, Spain.

^{d)}Author to whom correspondence should be addressed: danielrodriguez@ugr.es

ABSTRACT

In this study, we report on the stabilization of a continuous-wave Ti:Sa laser to an optical frequency comb. The laser is emitting at 866 nm to address one of the transitions required for Doppler cooling of a single $^{40}\text{Ca}^+$ ion in a linear Paul trap ($^2D_{3/2} \leftrightarrow ^2P_{1/2}$). The stabilized Ti:Sa laser is utilized to calibrate an ultra-accurate wavelength meter. We certify this self-reference laser source by comparing the results from monitoring the laser-cooled $^{40}\text{Ca}^+$ ion in the linear Paul trap, with those obtained when a HeNe laser is used for calibration. The use of this self-reference is compatible with the simultaneous use of the comb for precision spectroscopy in the same ion-trap experiment.

Published under an exclusive license by AIP Publishing. <https://doi.org/10.1063/5.0094452>

I. INTRODUCTION

Ion trap experiments for precision spectroscopy and quantum metrology^{1–5} require different degrees of stability in the lasers utilized to drive electronic transitions to cool an ion efficiently. Laser cooling is also a prerequisite to implement a single or multi-ion platform for sensing^{6,7} or computation.^{8,9} An example of a suitable cooling scheme comprises two consecutive steps (see Ref. 10 for a review and Ref. 11 for $^{40}\text{Ca}^+$). The first step, called Doppler cooling, uses an electric-dipole transition with a linewidth of ≈ 20 MHz and allows reaching an ion temperature in the order of an mK. The second step, known as sideband cooling, uses a quadrupole transition with a linewidth below 1 Hz, to drive the ion to its ground state of motion.

For electric-dipole transitions, the laser frequencies can be regulated with the required precision and accuracy using wavelength meters (WLM) based on multiple solid Fizeau interferometers.¹² They can provide wavelength measurements of the lasers involved, sequentially, with a typical time of about 10 ms per single measurement, with absolute accuracies down to 2 MHz in a broad spectrum ranging from the IR to the near UV. The wavelengths of the different lasers involved in the experiments are measured sequentially, and the laser source is adapted to provide the desired frequency in each case. The performance of such devices in terms of stability and accuracy has been thoroughly analyzed in a large variety of laser-spectroscopy experiments.^{13–17} Fluctuations of the ambient conditions induce drifts that must be compensated to maintain the accuracy and reproducibility of the wavelength measurements over

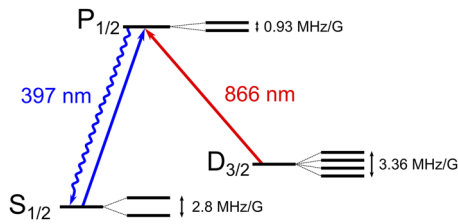


FIG. 1. Energy-level structure of the $^{40}\text{Ca}^+$ ion in the presence of a magnetic field. The solid-straight arrows indicate the transitions used to perform Doppler cooling (blue) and repumping of the metastable $D_{3/2}$ state (red).

long time scales. These long-term drifts can be corrected by a regular calibration of the WLM with an absolute-reference laser source such as, e.g., a frequency-stabilized HeNe laser, which offers relative accuracies in the order of 5×10^{-9} . For a dipole-forbidden transition, the laser is locked to a high-finesse cavity, and the frequency can be accurately measured with an optical frequency comb.^{18,19} Optical frequency measurements with combs can achieve relative accuracies better than 8×10^{-12} when the comb is locked to a GPS reference. Besides this regular comb application, exploited in quantum metrology ion-trap based measurements,^{2,3} the comb can serve in the same experiment for the stabilization of a laser source with a linewidth of a few hundred kHz, providing a self-reference for the WLM from an atomic dipole-transition, at the time this source drives it in the experiment.

In this publication, we demonstrate the frequency stabilization of a continuous-wave titanium:sapphire (Ti:Sa) ring laser emitting at $\lambda = 866$ nm locked to an optical frequency comb, and its use in a Doppler cooling experiment. We compare the frequency stability of the Ti:Sa laser with that obtained when this is stabilized by means of a WLM calibrated with a HeNe laser. We find that the measurement uncertainty when locking to the comb is closer to the achievable linewidth of the laser beam in our experiment. This use of the Ti:Sa laser as a suitable self-reference has been certified experimentally in this work by observing a single laser-cooled $^{40}\text{Ca}^+$ ion stored in a linear Paul trap. While in this experiment only three lasers are needed, the WLM-based regulation using the self-reference source can be applied for Doppler cooling of a calcium ion or an unbalanced two-ion crystal in a 7 T Penning trap^{20–23} where, in addition to the Ti:Sa laser, eight tunable diode lasers have to be stabilized. The level scheme for $^{40}\text{Ca}^+$ is shown in Fig. 1 where the transitions for Doppler cooling ($\lambda = 397$ nm) and repumping of the metastable $D_{3/2}$ state ($\lambda = 866$ nm) are indicated by solid arrows. The figure also shows the Zeeman splittings per magnetic field strength.

II. EXPERIMENTAL SETUP

A. The Ti:Sa laser regulation system

The full system for regulation and the experimental setup is depicted in Fig. 2. In the experiments presented in this manuscript, the laser is used to pump the $^2D_{3/2} \leftrightarrow ^2P_{1/2}$ transition. The 866 nm laser light is generated by a Ti:Sa ring laser (Sirah Matisse TX) that is pumped by a 532 nm diode-pumped solid-state laser (Spectra Physics Millennia eV-15 W). The ring cavity is built with several

frequency-selective elements to ensure single-mode operation in a broad wavelength spectrum. The Ti:Sa laser is frequency-stabilized to an external cavity with finesse $\mathcal{F} \approx 400$ using the Pound-Drever-Hall (PDH) technique. The laser system requires an additional lock to a stable reference in order to avoid long-term drifts of the frequency arising from the ambient conditions of the external cavity. As shown in Fig. 2, two references are available in our laser setup for this purpose. One approach, marked as WLM 1, involves the use of a commercial, high-precision WLM (HighFinesse WS8) as the reference. A fraction of the laser output is guided through a single-mode (SM) fiber and in-coupled to the WLM via a multi-channel fiber switch. The switch is coupled to the WLM by means of a photonic-crystal fiber, allowing us to perform the simultaneous readout and stabilization of up to eight laser sources over the standard spectral range (330–1180 nm). In these conditions, the device has a specified measurement resolution of 0.4 MHz and a specified absolute accuracy of ± 10 MHz. The readout time for each channel is in the order of 10 ms, and the corresponding wavelengths are displayed using the HighFinesse proprietary software on a computer (PC-1 in Fig. 2) that is linked to the WLM via a universal serial bus (USB) connection. The Ti:Sa laser controller is connected to PC-1 via USB and graphically interfaced by means of the LabVIEW-based control software provided by the manufacturer. An application library of this software, denoted as plug-in, allows the readout from the WLM to be integrated into the control software as an input value for a built-in proportional-integrative-derivative (PID) controller that regulates the lock of the laser to the reference. In this manner, the digital frequency readout is processed as an analog control signal that is sent to a piezoelectric actuator in the external cavity that compensates for the long-term drifts and an intra-cavity EOM that performs fast corrections of the laser frequency (~ 1 MHz bandwidth). This stabilization scheme has been employed in previous experiments with a different number of lasers.^{20,24–26} In those experiments, a HeNe laser (SIOS Meßtechnik SL 03) with a specified accuracy of ± 5 MHz was used for calibration of the WLM.

Alternatively, as presented in this manuscript, an optical frequency comb (Menlo Systems FC1550-250-WG) has been utilized as the reference for the lock of the Ti:Sa laser system. The frequency comb has a regular mode spacing of 250 MHz and is locked to a 10 MHz reference signal produced by a GPS-disciplined, oven-controlled quartz oscillator (Menlo Systems GPS 8–12) with a specified frequency stability better than 8×10^{-12} in 1 s. The corresponding setup is marked as Frequency Comb 2 in Fig. 2, where a fraction of the laser output is guided through a SM fiber and superimposed with the frequency comb. The beat note frequency between the Ti:Sa laser and the nearest comb tooth is detected with a fast photodiode (Menlo Systems APD210) and processed using any of the schemes shown in Fig. 3. The beat note at 60 MHz is detected, band-pass filtered, and amplified inside the oscillation frequency detection (OFD) unit. Afterward, the beat note signal is split into two branches. One goes directly to a frequency counter (K+K Meßtechnik FXM50) with an integration time of one second (2.1 in Fig. 3). The frequency counter is connected to a computer (PC-2 in Fig. 2) via RS232 link for data logging with a fixed sampling time of 1 s. Among other parameters, the absolute laser frequency can be calculated and recorded by means of the proprietary control software. PC-2 is linked to PC-1 via a local area network (LAN) connection, hence the digital frequency readout can be implemented

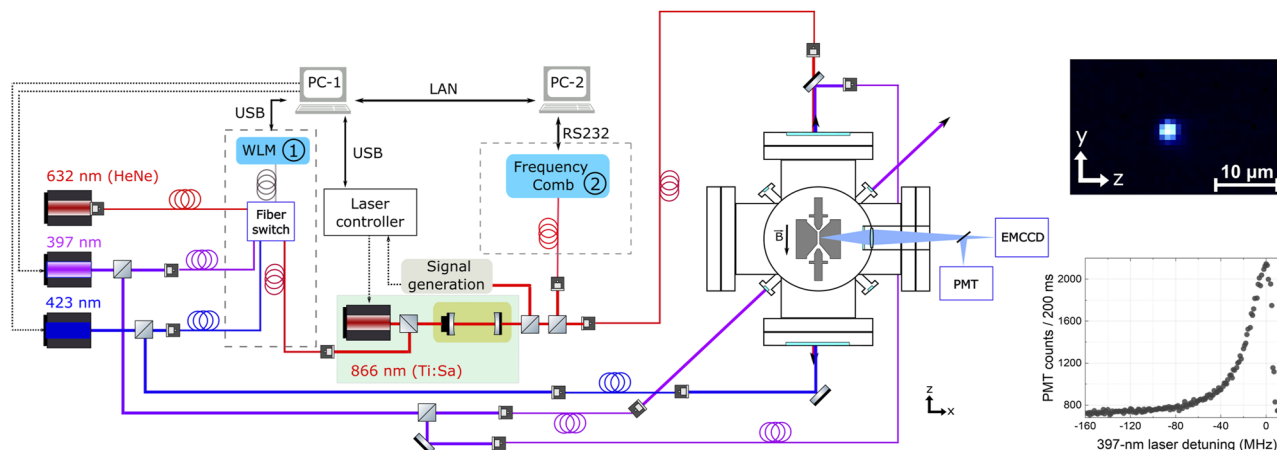


FIG. 2. Schematic of the experimental setup to perform Doppler cooling on a single laser-cooled ion with a stabilization system for a Ti:Sa laser by means of a WLM (marked as 1) or a frequency comb (marked as 2). Both setups provide the frequency measurement and locking by sending a fraction of the laser output through a single-mode (SM) fiber. In 1, the wavemeter is calibrated using a HeNe laser, while in 2 uses the outcome from the frequency comb stabilization. The image of a single laser-cooled ion on an EMCCD sensor, as well as the photons signal obtained with a PMT as a function of the 397 nm laser frequency, is shown on the right. More details are given in the text.

into the laser stabilization setup across the local network. A custom-made plug-in developed in this work integrates the frequency comb readout into the laser control software in the same fashion as the aforementioned lock to the WLM.

Furthermore, a frequency divider unit (FDT) can be used to reduce the readout time when the lock to the comb is engaged

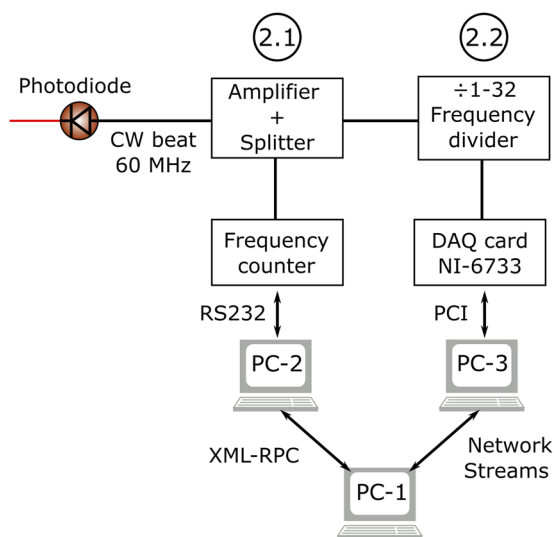


FIG. 3. Schematic of the layout of the Ti:Sa laser frequency stabilization using a frequency comb. The beat note frequency is detected and split into a frequency counter and a frequency divider unit (FDT). One approach (marked as 2.1) uses the frequency readout from the frequency counter with an acquisition time of 1 s. Alternatively, another approach (marked as 2.2) uses the output of the FDT whose frequency is counted by a NI-DAQ card. Both setups are linked to PC-1 via LAN connection using different communication protocols.

(2.2 in Fig. 3). The unit is part of the electronics used to lock the repetition rate to an optical reference (e.g., ultra-stable laser). The signal going to the FDT is divided by an adjustable integer ranging from 1 to 32. One of the available output ports of the FDT is connected to a DAQ card (NI PIC-6733) to perform the readout of the divided beat note frequency. The card has a two-counter feature providing a fast 24-bit digital readout that can be integrated into the PID regulation of the Ti:Sa laser. Since maximum input frequency of the DAQ card is 20 MHz, we divide the beat note frequency down to 2 MHz by setting a factor of 30 at the divider. This frequency readout is further processed to yield the absolute frequency of the Ti:Sa laser with a sampling time of nearly 230 ms. We observed no differences between both configurations from the respective frequency stability measurements. Thus, the configuration 2.1 has been used for the experiments presented in this manuscript.

B. The linear Paul trap

The configuration of the linear Paul trap is based on the design developed at the University of Innsbruck.^{27,28} The trap consists of four blade-shaped electrodes, where a time-varying quadrupolar field is applied to provide confinement in the radial plane, and two endcap electrodes to which a DC voltage is applied for axial confinement. A top view of the trap (not to scale) inside the vacuum chamber is shown in Fig. 2, where two of the four blade-shaped electrodes and the endcaps are visible (x - z plane). A magnetic field of $B = 4$ G is generated along the axial direction by a pair of coils (not shown). The background pressure is around 3×10^{-11} mbar. The radiofrequency (RF) of the time varying field is 21.9 MHz and the amplitude of the RF voltage gives rise to a radial oscillation frequency $\omega_r = 2\pi \times 1.75$ MHz. The potential applied to the endcaps results in an axial oscillation frequency of $\omega_z = 2\pi \times 1.022$ MHz. The $^{40}\text{Ca}^+$ ion is loaded into the trap by isotope-selective photoionization of neutral calcium atoms, which is accomplished by means of a tunable and a free-running diode lasers at wavelengths of 423

and 375 nm, respectively. The 397 nm photons scattered by the ion are collected by means of an objective with a numerical aperture of 0.34 (Sill Optics S6ASS2241). The objective is located in an inverted view port at a working distance of 58 mm from the trap center and provides a magnification factor of $\times 20$. The fluorescence image is recorded using an Electron Multiplying Charge-Coupled Device (EMCCD) camera, the sensor of which is placed at the focal plane. A beam splitter placed in front of the EMCCD camera diverts half of the fluorescence to a Photomultiplier Tube (PMT) to count the 397 nm photons. The top right of Fig. 2 shows the image of a single laser-cooled $^{40}\text{Ca}^+$ ion recorded with the EMCCD when the experiment is running under optimal conditions. The bottom right of Fig. 2 shows the fluorescence photons recorded by the PMT as a function of the 397 nm laser frequency.

The 397 nm laser is split in two beam paths, one directed parallel to $-\hat{k}$ (z direction) and the other in the direction with unitary vector $(\hat{i} + \hat{k})/\sqrt{2}$, with a power of 225 and 13 μW , respectively. The spot size of the lasers (I_{max}/e^2) is 220 μm (axial) and 190 μm (radial-axial). The axial beam, with a saturation parameter $s \approx 4-5$, has been only used while loading the ion in the trap. The other 397 nm beam, with $s = 0.8$, is present all the time during the measurements reported here. The 866 nm laser beam is directed along the z direction with an intensity above saturation. For all the measurements, the excess micromotion^{29,30} has been compensated using the two techniques that were within our reach. We performed the minimization of the spatial displacement of the ion, monitored with the EMCCD camera, as the RF voltage is varied²⁷ and the minimization of the measured width of the $^2\text{S}_{1/2} \leftrightarrow ^2\text{P}_{1/2}$ cooling transition when the 397 nm laser frequency is scanned across the resonance.²⁸

III. EXPERIMENTAL RESULTS

The experiments reported here are devoted to lock and stabilize the 866 nm repumper laser needed for Doppler cooling of a single $^{40}\text{Ca}^+$ ion using a frequency comb. The 397 and 423 nm laser frequencies were stabilized using the WLM and a built-in PID module integrated into the HighFinesse software. To avoid drifts of the WLM readout due to ambient temperature fluctuations, the WLM was calibrated with a reference laser through a calibration feature of the software. Since readout of each channel of the fiber switch takes a few tens of ms, a complete measurement cycle of the WLM takes 110 ms while for the frequency comb it takes 1 s to measure the 866 nm laser frequency. Figure 4 shows the temporal variations of the 866 nm laser frequency measured with the frequency comb for the two locking schemes. The left side of Fig. 4 shows the frequency drift when the 866 nm laser is stabilized to the WLM. Here, the WLM is calibrated with the HeNe laser using the reference value provided by the manufacturer ($\nu_{\text{calibration}} = 473.612\,462(5)$ THz). The right side of Fig. 4 shows the frequency drift when the 866 nm laser is stabilized to the comb, using the optical beat note between the laser and the nearest comb tooth. In this scenario, we measured an FWHM linewidth of 654(2) kHz for the optical beat note measured with a resolution bandwidth of 100 kHz, when the laser was tuned to the resonance of the $^2\text{D}_{3/2} \leftrightarrow ^2\text{P}_{1/2}$ transition ($\lambda = 866$ nm), which in turn serves as the reference value to calibrate the WLM ($\nu_{\text{calibration}} = 346.000\,241$ THz). This FWHM linewidth is larger than 476(4) kHz, obtained when the WLM is calibrated with the HeNe

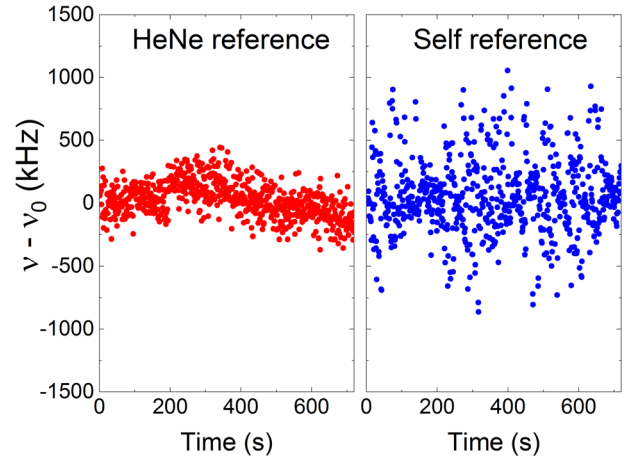


FIG. 4. Frequency drift of the 866 nm laser during the measurements carried out using a single laser-cooled ion in the linear Paul trap. Left: the WLM, which regulates the 397 nm and 423 nm lasers, is calibrated using the HeNe laser as the reference. Right: the WLM is calibrated with the 866 nm laser frequency that drives the $^2\text{D}_{3/2} \leftrightarrow ^2\text{P}_{1/2}$ transition in $^{40}\text{Ca}^+$. This self-reference is locked to the comb.

laser. In both cases, the calibration of the WLM is performed every 3 min.

To characterize the relative frequency stability of both references, we have computed the Allan deviation from the measured frequencies shown in Fig. 4. The Allan deviation σ_y is given by³¹

$$\sigma_y^2(\tau) = \frac{1}{2m^2(M-2m+1)} \sum_{j=1}^{M-2m+1} \sum_{i=j}^{j+m-1} (y_{i+m} - y_i)^2, \quad (1)$$

where y is the fractional frequency, given by $(\nu - \nu_0)/\nu_0$ with ν_0 being the nominal frequency. M is the number of samples, and τ is the averaging time, which is defined as $\tau = m\tau_0$, where m is the average time factor and τ_0 is the sampling time.

The computed Allan deviations are presented in Fig. 5. When the WLM serves as the reference for the 866 nm laser and is calibrated by the HeNe laser (red curve), the Allan deviation follows a $3 \times 10^{-10} \tau^{-1/2}$ dependency for $1 < \tau < 16$ s and decreases down to a minimum of 7.5×10^{-11} at $\tau = 16$ s. The Allan deviation then increases up to a maximum of 1.8×10^{-10} at 128 s, following a $1.7 \times 10^{-11} \tau^{1/2}$ dependency for $16 < \tau < 128$ s. When the WLM is calibrated by the self-reference (blue curve), the Allan deviation follows a $7 \times 10^{-10} \tau^{-1/2}$ dependency for $8 < \tau < 128$ s and decreases down to a minimum of 7.7×10^{-11} at $\tau = 128$ s. We find a bump around $\tau = 2$ s that yields a maximum Allan deviation of 7.5×10^{-10} . This bump arises from sudden frequency jumps in the 866 nm laser that can be seen as outliers with amplitudes higher than 500 kHz in Fig. 4 (right side) and may be interpreted as a periodic, burst noise-like perturbation that is not compensated by the PID regulation of the Ti:Sa laser. The exact origin of the frequency jumps in the self-reference remains unclear. All in all, in both scenarios the Allan deviation is better than 1×10^{-9} over the integration times considered here. We also observe that the self-reference gives a better relative stability for $\tau > 40$ s compared to the HeNe calibration of the WLM.

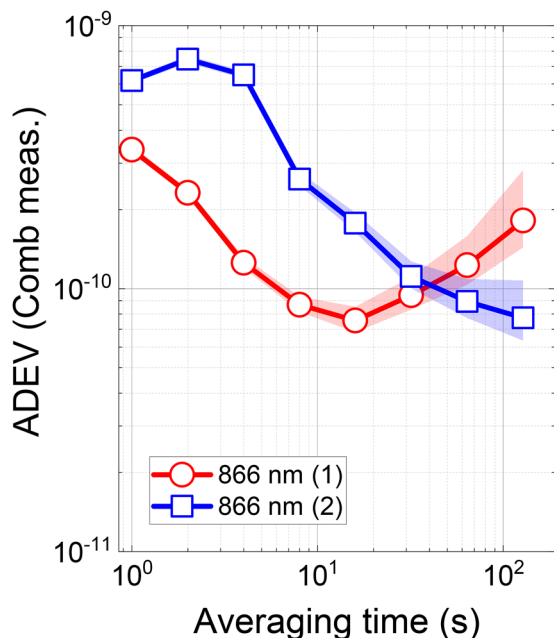


FIG. 5. Comparison of the computed Allan deviations [Eq. (1)] from the measurements shown in Fig. 4. We compare two configurations: (1) The Ti:Sa laser is regulated with the WLM, in turn, calibrated with a HeNe laser; (2) the Ti:Sa laser is locked to the comb and serves as a reference to calibrate the WLM.

On the other hand, a single laser-cooled $^{40}\text{Ca}^+$ ion was stored in the linear Paul trap, and the cooling transition was probed by scanning the 397 nm laser frequency while the 866 nm laser frequency was stabilized and measured as depicted in Fig. 4. The fluorescence photons were recorded with the PMT to obtain resonance spectra as the one shown in the bottom right of Fig. 2. For the measurements presented here, the compensation voltages were adjusted in order to minimize the width of the fluorescence spectrum. Figure 6 depicts the compensation process. We scan the 397 nm laser frequency for different compensation voltages, and we find a minimum width of 23.0 ± 0.7 MHz for $V_{\text{comp}} = -50$ V. To determine the width of the spectrum, we use a Voigt profile as the fitting function that accounts for the Doppler broadening of the spectrum due to the ion motion in the trap. The width of the Lorentzian profile is fixed to 22.4 MHz, which is the natural linewidth of the $^2\text{S}_{1/2} \leftrightarrow ^2\text{P}_{1/2}$ cooling transition. The Lorentzian is obtained by summing over the four possible $^2\text{S}_{1/2}(m) \leftrightarrow ^2\text{P}_{1/2}(m')$ transitions between the respective Zeeman sublevels ($m, m' = \pm 1/2$) that arise due to the magnetic field applied in the experiment (see Fig. 1). The Gaussian widths were obtained by fitting the Voigt function to each of the recorded spectra.

The subsequent measurements of the spectra for a single-ion (SI) using both references as the calibration source of the WLM are shown in Fig. 7. From the SI data, we obtain an average Gaussian FWHM of 25.8 ± 4.4 MHz for the HeNe calibration and 26.7 ± 4.1 MHz for the self-reference calibration. The temperature deduced from these measurements in both cases is nearly a factor of 60 greater than the temperature in the Doppler limit for a saturation parameter of $s = 0.8$ ($T_D \approx 0.7$ mK), the latter corresponding to a Gaussian

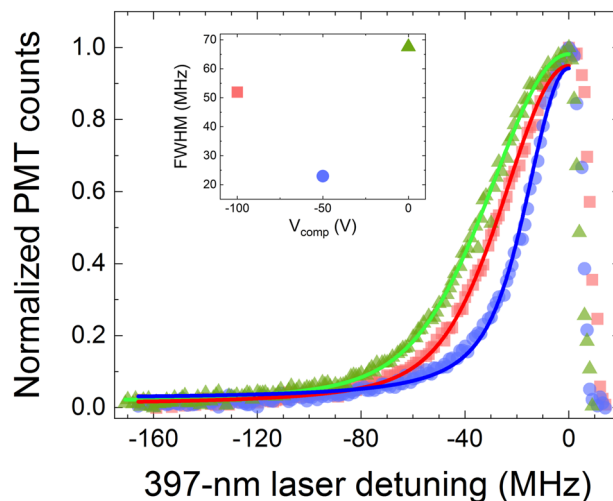


FIG. 6. Excess micromotion compensation using the $^2\text{S}_{1/2} \leftrightarrow ^2\text{P}_{1/2}$ cooling transition. The spectra are obtained by scanning the 397 nm laser frequency across resonance for compensation voltages of 0 V (green), -50 V (blue), and -100 V (red). The inset shows the Gaussian widths (FWHM) obtained from the Voigt fit to the spectra, where we find a minimum width of ~ 20 MHz for $V_{\text{comp}} = -50$ V.

FWHM of 3.2 MHz. The difference between expected temperature and observed temperature can be explained from the experimental method employed here for spectroscopy of the $^2\text{S}_{1/2} \leftrightarrow ^2\text{P}_{1/2}$ cooling transition, which introduces systematic effects that limit its accuracy to determine the temperature of the ion. The 397 nm laser frequency determines the cooling rate and, thus, the final temperature of the ion in equilibrium.¹⁰ Hence, the scanning of this frequency

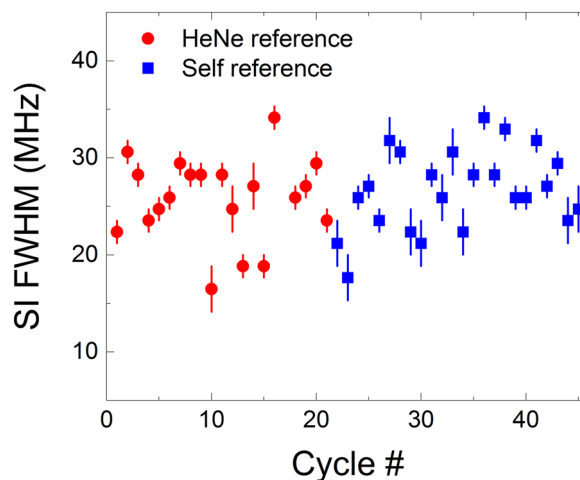


FIG. 7. Gaussian widths (FWHM) extracted from the Voigt fit to the fluorescence profiles of a Single-Ion (SI) while using the HeNe reference (red circles) and the self-reference (blue squares). The profiles are obtained by scanning the 397 nm laser across resonance. The Lorentzian width is fixed to $\Gamma/2\pi = 22.4$ MHz. See text for more details.

perturbs the laser cooling dynamics during the spectroscopy measurements and, consequently, the effective width of the spectrum broadens. In addition, the simultaneous presence of the 397 and 866 nm beams during the experiment complicates the structure of the ideal two-level system and leads to an effective broadening of the spectrum that depends on multiple parameters of both laser beams, as well as the intensity and orientation of the magnetic field.³² Thus, the uncertainties derived from this effect must be evaluated by solving the Bloch equations for the complete eight-level system,³³ where the effect of micromotion should be taken into account.³⁴ Our hypothesis is reinforced since we have determined the temperature under similar conditions through the spectroscopy of the electric-quadrupole transition of $^{40}\text{Ca}^+$ at 729 nm and we have obtained temperature values that are lower by more than an order of magnitude compared to the results presented above. This method has been recently introduced in our experimental setup and it is described in detail in the [Appendix](#) of the manuscript. Thus, the temperature values of $T_{\text{HeNe}} = 46 \pm 15$ mK and $T_{\text{self}} = 49 \pm 15$ mK obtained from [Fig. 7](#) should be interpreted as an upper limit due to the measurement procedure and suggest that the performance of the Doppler cooling (and the perturbation introduced by the measurement technique) of a $^{40}\text{Ca}^+$ ion in a linear Paul trap is equivalent using both references as the calibration source.

IV. CONCLUSIONS AND OUTLOOK

In this work, a Ti:Sa laser emitting at $\lambda = 866$ nm to pump the metastable state $D_{3/2}$ in $^{40}\text{Ca}^+$ has been locked to a frequency comb using a custom plug-in software developed in our laboratory. We demonstrate that this locking scheme also provides a self-reference to calibrate a high-precision WLM for reliable operation over long timescales. The self-reference has been tested as a reference for the long-term stabilization of several laser sources in Doppler cooling experiments with a single $^{40}\text{Ca}^+$ ion stored in a linear Paul trap. The experiment using the self-reference has been compared with an analogous experiment that employs a HeNe laser as the reference. We characterized a relative frequency stability better than 1×10^{-9} between integration times of 1 and 128 s for this experiment. We measured the variation of the fluorescence photons with the frequency of the 397 nm laser beam, scanned across resonance, and we conclude that both schemes are suitable when the Doppler cooling experiment is run under the optimal attainable conditions. This stabilization scheme opens the possibility to use the optical frequency comb as the reference in more complex scenarios involving many laser sources,³⁵ as it happens when the laser-cooled $^{40}\text{Ca}^+$ ion is stored in a Penning trap located in a magnetic field of 7 T,²⁰ where up to eight more diode lasers are required for Doppler cooling. Furthermore, under minor modifications in the comb setup, this can be simultaneously used to measure accurately the frequency of the quadrupole transition $^2S_{1/2} \leftrightarrow ^2D_{5/2}$ in $^{40}\text{Ca}^+$.

ACKNOWLEDGMENTS

We acknowledge support from the Spanish MICINN through Project No. PID2019-104093GB-I00/AEI/10.01339/501100011033 and Contract No. PTA2018-016573-I, from the Andalusia Government through Project No. P18-FR-3432 and Fondo

Operativo FEDER A-FQM-425-UGR18, from the Spanish Ministry of Education through the Ph.D. fellowship under Grant No. FPU17/02596, and from the University of Granada “Plan propio—Programa de Intensificación de la Investigación,” Project No. PP2017-PRI-I-04 and “Laboratorios Singulares 2020.” The construction of the facility was supported by the European Research Council (Contract No. 278648-TRAPSENSOR), Project Nos. FPA2015-67694-P and FPA2012-32076, Infrastructure Project Nos. UNGR10-1E-501, UNGR13-1E-1830, and EQC2018-005130-P (MICINN/FEDER/UGR), and Grant Nos. IE-5713 and IE2017-5513 (Junta de Andalucía-FEDER). J.C. acknowledges support from the Spanish MICINN (“Beatriz Galindo” Fellowship, Grant No. BEAGAL18/00078).

AUTHOR DECLARATIONS

Conflict of Interest

The authors have no conflicts to disclose.

Author Contributions

F. Domínguez: Formal analysis (lead); Investigation (lead); Methodology (lead). **J. Bañuelos:** Resources (equal); Software (equal). **J. Berrocal:** Investigation (equal); Resources (equal). **J. J. Del Pozo:** Investigation (equal); Software (equal). **M. Hernández:** Investigation (equal). **A. Carrasco-Sanz:** Investigation (equal). **J. Cerrillo:** Investigation (equal). **P. Escobedo-Araque:** Investigation (equal); Software (equal). **D. Rodríguez:** Formal analysis (supporting); Funding acquisition (lead); Investigation (lead); Methodology (equal); Project administration (lead); Supervision (lead).

DATA AVAILABILITY

The data that support the findings of this study are available from the corresponding author upon reasonable request.

APPENDIX: ION TEMPERATURE DETERMINATION USING OPTICAL SIDEBAND SPECTROSCOPY OF THE 729 nm TRANSITION

As stated in [Sec. III](#), the spectroscopy method employed there to probe the electric-dipole $^2S_{1/2} \leftrightarrow ^2P_{1/2}$ cooling transition poses several limitations that prevent the accurate determination of the effective linewidth, and, thus, the final temperature of the ion. To circumvent these limitations, several methods have been implemented in order to perform more accurate spectroscopy on electric-dipole transitions in $^{40}\text{Ca}^+$ via fast switching of the 397 and 866 nm beams.^{34,36–38} However, the most accurate measurements can be performed through the spectroscopy on the narrow electric-quadrupole $^2S_{1/2} \leftrightarrow ^2D_{5/2}$ transition at 729 nm (natural linewidth of $\Gamma_{729}/2\pi = 0.136$ Hz). In this manner, accurate measurements of the temperature of the ion can be performed in experiments with $^{40}\text{Ca}^+$ stored in Paul³⁹ and Penning traps⁴⁰ that allow one to determine whether the Doppler limit was achieved.

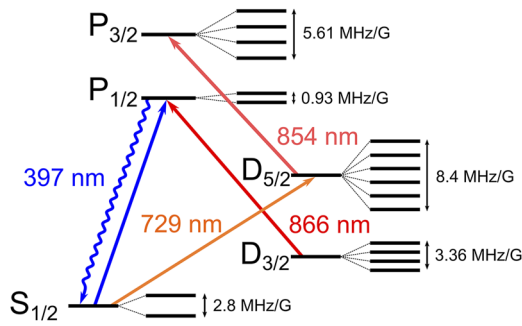


FIG. 8. Level scheme of the $^{40}\text{Ca}^+$ ion for optical sideband spectroscopy in the presence of a magnetic field. The solid-straight arrows indicate the transitions used to perform Doppler cooling (blue), repumping of the $D_{3/2}$ state (red), “quenching” of the $D_{5/2}$ state (light red), and sideband spectroscopy (orange).

The level scheme for the spectroscopy of $^2S_{1/2} \leftrightarrow ^2D_{5/2}$ in $^{40}\text{Ca}^+$ is depicted in Fig. 8. The transitions employed for Doppler cooling ($\lambda = 397$ nm), repumping of the $D_{3/2}$ state ($\lambda = 866$ nm), quenching of the $D_{5/2}$ state ($\lambda = 854$ nm), and spectroscopy ($\lambda = 729$ nm) are indicated by solid arrows. In these measurements, an ultra-stable and narrow 729 nm laser is scanned across the resonance of the $^2S_{1/2} \leftrightarrow ^2D_{5/2}$ transition. Since resolved-sideband regime is achieved here, the absorption spectrum of this transition exhibits multiple sidebands around the resonance that is located at the oscillation frequencies of the ion, as opposed to the continuous Doppler-broadened profile that we observe in the scans of the 397 nm laser frequency presented in Sec. III.

In a recent extension of our experimental setup, we have installed a 729 nm tapered amplifier laser diode that is locked to a high-finesse cavity in order to drive the electric-quadrupole $^2S_{1/2} \leftrightarrow ^2D_{5/2}$ transition. The lock to the cavity is engaged using the PDH technique, where we measured a finesse $\mathcal{F} \approx 270\,000$ and a long-term linear drift of 330 mHz/s. The 729 nm laser beam is directed to the ion along the z direction, co-propagating with the 866 and 397 nm (axial) laser beam paths described in Sec. II and shown in Fig. 2. A pulsed 854 nm laser beam was also directed along the z direction and frequency-stabilized using the PID module from HighFinesse mentioned in Sec. III to “quench” the $D_{5/2}$ level for the spectroscopy measurements presented here. In our setup, we address the $^2S_{1/2}(m = -1/2) \leftrightarrow ^2D_{5/2}(m' = -3/2)$ transition out of the 10 possible transitions between the $S_{1/2}$ and $D_{5/2}$ sublevels that arise from the presence of the magnetic field (see Fig. 8).

The absorption spectrum is obtained with a pulsed spectroscopy sequence that makes use of the “quantum jump” technique.⁴¹ The resulting absorption spectrum for the axial motion is shown in Fig. 9. It corresponds to that of a thermal state, which consists of an evenly spaced comb of sidebands modulated by a Gaussian envelope that accounts for the residual Doppler broadening.⁴² Therefore, in this scenario, the fitting function is given by the product between a Lorentzian comb of evenly spaced sidebands and a Gaussian envelope. The fit to the data yields a value of 2.4 ± 0.2 MHz for the Gaussian FWHM. This corresponds to a temperature of $T = 1.4 \pm 0.3$ mK, which implies a mean occupation number of $\bar{n}_z = 28 \pm 5$ for the axial motion. This value is nearly 2 times greater than the Doppler limit, where we would expect a temperature of

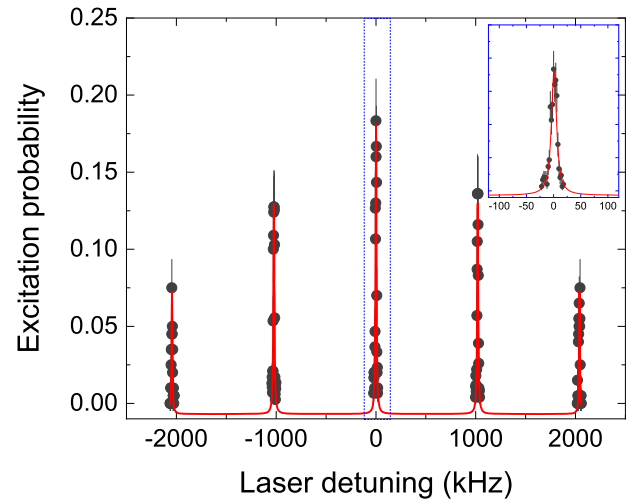


FIG. 9. Experimental spectrum showing the sidebands at the axial oscillation frequency of 1.022 MHz. The spectrum is windowed around the expected sidebands to reduce the acquisition time. The inset shows the window corresponding to the resonance frequency scan of the $^2S_{1/2} \leftrightarrow ^2D_{5/2}$ transition, which is enclosed with blue dashed lines in the main plot. The frequency span was 40 kHz and the frequency step was 2 kHz for each window. The fit (red curve) is the product of a symmetric Lorentzian comb and a Gaussian envelope.

$T_D \approx 0.7$ mK (FWHM ≈ 1.77 MHz) and a mean occupation number of $\bar{n}_z \approx 15$ for an axial oscillation frequency of 1.022 MHz in the trap. The discrepancy may be explained by the effects of saturation due to excessive power of the laser beams still, or an inaccurate adjustment of the 397 nm laser frequency, which should be red-detuned by $\Delta_{397} = (\Gamma_{397}/2\pi)\sqrt{s+1}/2$ from the resonance to achieve the Doppler limit. All things considered, the spectroscopy on the electric-quadrupole transition at 729 nm described here provides an accurate and reliable method to evaluate the performance of the Doppler cooling in the experiments presented in this manuscript.

REFERENCES

- P. O. Schmidt, T. Rosenband, C. Langer, W. M. Itano, J. C. Bergquist, and D. J. Wineland, *Science* **309**, 749 (2005).
- T. Rosenband, D. B. Hume, P. O. Schmidt, C. W. Chou, A. Brusch, L. Lorini, W. H. Oskay, R. E. Drullinger, T. M. Fortier, J. E. Stalnaker, S. A. Diddams, W. C. Swann, N. R. Newbury, W. M. Itano, D. J. Wineland, and J. C. Bergquist, *Science* **319**, 1808 (2008).
- M. Chawalla, J. Benhelm, K. Kim, G. Kirchmair, T. Monz, M. Riebe, P. Schindler, A. S. Villar, W. Hänsel, C. F. Roos, R. Blatt, M. Abgrall, G. Santarelli, G. D. Rovera, and P. Laurent, *Phys. Rev. Lett.* **102**(2), 023002 (2009).
- F. Wolf, C. Shi, J. C. Heip, M. Gessner, L. Pezzè, A. Smerzi, M. Schulte, K. Hammerer, and P. O. Schmidt, *Nat. Commun.* **10**, 2929 (2019).
- P. Micke, T. Leopold, S. A. King, E. Benkler, L. J. Spiess, L. Schmöger, M. Schwarz, J. R. Crespo López-Urrutia, and P. O. Schmidt, *Nature* **578**, 60 (2020).
- M. J. Biercuk, H. Uys, J. W. Britton, A. P. VanDevender, and J. J. Bollinger, *Nat. Nanotechnol.* **5**, 646 (2010).
- P. A. Ivanov, N. V. Vitanov, and K. Singer, *Sci. Rep.* **6**, 28078 (2016).
- J. I. Cirac and P. Zoller, *Phys. Rev. Lett.* **74**, 4091 (1995).
- N. Friis, O. Marty, C. Maier, C. Hempel, M. Holzpfel, P. Jurcevic, M. Plenio, M. Huber, C. Roos, R. Blatt, and B. Lanyon, *Phys. Rev. X* **8**, 021012 (2018).

- ¹⁰D. Leibfried, R. Blatt, C. Monroe, and D. Wineland, *Rev. Mod. Phys.* **75**, 281 (2003).
- ¹¹P. Schindler, D. Nigg, T. Monz, J. T. Barreiro, E. Martinez, S. X. Wang, S. Quint, M. F. Brandl, V. Nebendahl, C. F. Roos, M. Chwalla, M. Hennrich, and R. Blatt, *New J. Phys.* **15**, 123012 (2013).
- ¹²J. L. Gardner, *Appl. Opt.* **24**, 3570 (1985).
- ¹³J. Zhang, W. H. Yuan, K. Deng, A. Deng, Z. T. Xu, C. B. Qin, Z. H. Lu, and J. Luo, *Rev. Sci. Instrum.* **84**, 123109 (2013).
- ¹⁴K. Saleh, J. Millo, A. Didier, Y. Kersalé, and C. Lacroûte, *Appl. Opt.* **54**, 9446 (2015).
- ¹⁵L. Couturier, I. Nosske, F. Hu, C. Tan, C. Qiao, Y. H. Jiang, P. Chen, and M. Weidemüller, *Rev. Sci. Instrum.* **89**, 043103 (2018).
- ¹⁶M. Verlinde, K. Dockx, S. Geldhof, K. König, D. Studer, T. E. Cocolios, R. P. de Groote, R. Ferrer, Y. Kudryavtsev, T. Kieck, I. Moore, W. Nörtershäuser, S. Raeder, P. Van den Bergh, P. Van Duppen, and K. Wendt, *Appl. Phys. B* **126**, 85 (2020).
- ¹⁷K. König, P. Imgram, J. Krämer, B. Maaß, K. Mohr, T. Ratajczyk, F. Sommer, and W. Nörtershäuser, *Appl. Phys. B* **126**, 86 (2020).
- ¹⁸T. Udem, R. Holzwarth, and T. W. Hänsch, *Nature* **416**, 233–237 (2002).
- ¹⁹T. Fortier and E. Baumann, *Commun. Phys.* **2**, 153 (2019).
- ²⁰M. J. Gutiérrez, J. Berrocal, J. M. Cornejo, F. Domínguez, J. J. Del Pozo, I. Arrazola, J. Bañuelos, P. Escobedo, O. Kaleja, L. Lamata, R. A. Rica, S. Schmidt, M. Block, E. Solano, and D. Rodríguez, *New J. Phys.* **21**, 023023 (2019).
- ²¹M. J. Gutiérrez, J. Berrocal, F. Domínguez, I. Arrazola, M. Block, E. Solano, and D. Rodríguez, *Phys. Rev. A* **100**, 063415 (2019).
- ²²J. Berrocal, E. Altozano, F. Domínguez, M. J. Gutiérrez, J. Cerrillo, F. J. Fernández, M. Block, C. Ospelkaus, and D. Rodríguez, *Phys. Rev. A* **105**, 052603 (2022).
- ²³J. Cerrillo and D. Rodríguez, *Europhys. Lett.* **134**, 38001 (2021).
- ²⁴J. M. Cornejo, M. Colombano, J. Doménech, M. Block, P. Delahaye, and D. Rodríguez, *Rev. Sci. Instrum.* **86**, 103104 (2015).
- ²⁵F. Domínguez, I. Arrazola, J. Doménech, J. S. Pedernales, L. Lamata, E. Solano, and D. Rodríguez, *Sci. Rep.* **7**, 8336 (2017).
- ²⁶F. Domínguez, M. J. Gutiérrez, I. Arrazola, J. Berrocal, J. M. Cornejo, J. J. Del Pozo, R. A. Rica, S. Schmidt, E. Solano, and D. Rodríguez, *J. Mod. Opt.* **65**, 613 (2018).
- ²⁷S. Gulde, “Experimental realization of quantum gates and the Deutsch-Josza algorithm with trapped $^{40}\text{Ca}^+$ ions,” Ph.D. thesis, University of Innsbruck, 2003.
- ²⁸C. Hempel, “Digital quantum simulation, Schrödinger cat state spectroscopy and setting up a linear ion trap,” Ph.D. thesis, University of Innsbruck, 2014.
- ²⁹D. J. Berkeland, J. D. Miller, J. C. Bergquist, W. M. Itano, and D. J. Wineland, *J. Appl. Phys.* **83**, 5025 (1998).
- ³⁰J. Keller, H. L. Partner, T. Burgermeister, and T. E. Mehlstäubler, *J. Appl. Phys.* **118**, 104501 (2015).
- ³¹W. J. Riley, *Handbook of Frequency Stability Analysis* (NIST, 2007).
- ³²D. J. Berkeland and M. G. Boshier, *Phys. Rev. A* **65**, 033413 (2002).
- ³³H. Oberst, “Resonance fluorescence of single barium ions,” M.Sc. thesis, University of Innsbruck, 1999.
- ³⁴T. Sikorsky, Z. Meir, N. Akerman, R. Ben-shlomi, and R. Ozeri, *Phys. Rev. A* **96**, 012519 (2017).
- ³⁵A. Lešundák, T. M. Pham, M. Čížek, P. Obšil, L. Slodička, and O. Číp, *Opt. Express* **28**, 13091 (2020).
- ³⁶A. L. Wolf, S. A. van den Berg, C. Gohle, E. J. Salumbides, W. Ubachs, and K. S. E. Eikema, *Phys. Rev. A* **78**, 032511 (2008).
- ³⁷T. Pruttivarasin, M. Ramm, and H. Häffner, *J. Phys. B: At., Mol. Opt. Phys.* **47**, 135002 (2014).
- ³⁸J. Roßnagel, K. N. Tolazzi, F. Schmidt-Kaler, and K. Singer, *New J. Phys.* **17**, 045004 (2015).
- ³⁹H. C. Nägerl, C. Roos, D. Leibfried, H. Rohde, G. Thalhammer, J. Eschner, F. Schmidt-Kaler, and R. Blatt, *Phys. Rev. A* **61**, 023405 (2000).
- ⁴⁰S. Mavadia, G. Stutter, J. F. Goodwin, D. R. Crick, R. C. Thompson, and D. M. Segal, *Phys. Rev. A* **89**, 032502 (2014).
- ⁴¹W. Nagourney, J. Sandberg, and H. Dehmelt, *Phys. Rev. Lett.* **56**, 2797 (1986).
- ⁴²D. J. Wineland and W. M. Itano, *Phys. Rev. A* **20**, 1521 (1979).